JOURNAL OF GEOPHYSICAL RESEARCH, VOL. 113, B05314, doi:10.1029/2007JB005316, 2008

The structure of the base of the outer core inferred from seismic waves diffracted around the inner core

Zuihong Zou,[1] Keith D. Koper,[1] and Vernon F. Cormier[2]

Received 7 August 2007; revised 18 November 2007; accepted 15 January 2008; published 30 May 2008.

[1] We systematically searched for seismograms of waves diffracted around the inner core (PKP_{Cdiff}) from all the temporary seismic arrays with data currently available at the IRIS DMC, as well as some permanent regional seismic arrays including F-NET in Japan and GRF in Germany, to assemble the largest high-quality PKP_{Cdiff} database ever created. PKP_{Cdiff} waves preferentially sample the base of the outer core and so contain important clues about Earth structure in this region. We measured PKP_{DF}–PKP_{Cdiff} differential traveltimes and PKP_{Cdiff}/PKP_{DF} amplitude ratios in the distance range of 154°–160° and modeled the observations using grid searches and full wave theory synthetic seismograms. The optimum model found by fitting the differential traveltimes has relatively low velocity at the base of the outer core as in AK135, which is consistent with many previous traveltime studies. However, the optimum model found by fitting the amplitude ratios (PKP_{Cdiff}/PKP_{DF}) does not exhibit this feature, and instead is closer to PREM. The discrepancy may be explained by two likely causes. One is that small-scale topography or roughness on the ICB tends to scatter energy away from PKP_{Cdiff} waves by generating trailing coda waves. The other is that there exists a thin layer with relatively low Q at the base of the outer core. This might be expected if there are suspended solid particles at the base of the outer core, as proposed decades ago. Both mechanisms could generate smaller PKP_{Cdiff} amplitudes without significantly affecting PKP_{Cdiff} traveltimes.

Citation: Zou, Z., K. D. Koper, and V. F. Cormier (2008), The structure of the base of the outer core inferred from seismic waves diffracted around the inner core, *J. Geophys. Res.*, *113*, B05314, doi:10.1029/2007JB005316.

1. Introduction

[2] A large number of seismological studies have suggested that the region just above the inner core boundary (ICB) is distinct from the rest of the outer core. The layer about 400 km above the ICB was originally termed the F-layer and was characterized by a strong low velocity zone [*Jeffreys*, 1939]. Later Earth models, constructed with more accurate traveltime data, instead defined this as a region of increased velocity, and often included one or more first order discontinuities above the ICB [*Bolt*, 1962, 1964; *Adams and Randall*, 1964; *Sacks and Saa*, 1969]. Ultimately though, these model types were also discarded, as PKP precursors were reinterpreted as energy scattered from mantle heterogeneities near the core mantle boundary (CMB) [*Doornbos and Husebye*, 1972; *Cleary and Haddon*, 1972; *Haddon and Cleary*, 1974]. Hence modern reference Earth models universally have smoothly increasing velocities at the base of the outer core.

[3] There is still some uncertainty, however, about the steepness of the velocity gradient at the base of the outer core. This is important because the velocity gradient strongly constrains the density gradient in the Earth's core. If we assume the pressure derivative of the bulk modulus is constant (~3.5) in the outer core [*Anderson and Ahrens*, 1994], then the Bullen parameter η [*Bullen*, 1963], which is the ratio between the actual density gradient and the gradient corresponding to uniform composition, only depends on the velocity gradient. The widely used reference Earth model PREM [*Dziewonski and Anderson*, 1981] has the Bullen parameter $\eta \sim 1$ through the outer core, which implies a homogeneous, adiabatic medium.

[4] More recent reference Earth models, such as PREM2 [*Song and Helmberger*, 1995] and AK135 [*Kennett et al.*, 1995], have significantly lower velocity gradients at the base of the outer core, corresponding to Bullen parameters significantly higher than 1 (Figure 1). In other words, these models imply that near the base of the outer core density increases too quickly to be explained solely by compression, and some sort of change in chemistry or phase must occur. Interestingly, core dynamical studies suggested a slurry layer occupied by free-floating broken dendrites just above the ICB several decades ago [*Loper and Roberts*, 1978, 1981; *Loper*, 1978]. However, more recent studies consider a slurry of suspended particles unlikely to exist in the Earth and instead suggest that a thin mushy zone is more probable [*Bergman*, 2003; *Shimizu et al.*, 2005].

[5] Several other seismic studies have also reported velocity gradients at the base of the outer core that are

[1]Department of Earth and Atmospheric Sciences, Saint Louis University, St. Louis, Missouri, USA.

[2]Department of Physics, University of Connecticut, Storrs, Connecticut, USA.

0148-0227/08/2007JB005316$09.00

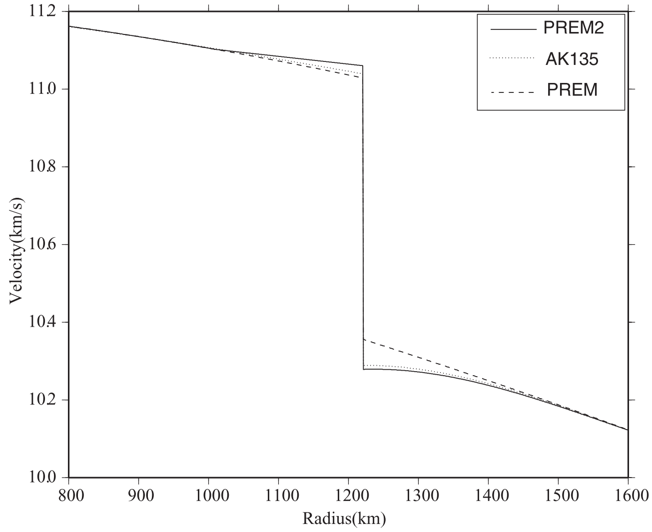

Figure 1. P wave velocity structure near the ICB. The radius of ICB in AK135 is shifted to be the same as PREM and PREM2. Dashed curve is for PREM, solid one is for PREM2 and dotted curve is for AK135. AK135 is nearly identical to PREM2 at the base of the outer core.

more similar to AK135 than to PREM. *Qamar* [1973] obtained a P wave velocity model named KOR5 with a very small gradient in the F-layer, and derived an η of 3–4. *Souriau and Poupinet* [1991] examined the *PKP*(*BC* + *Cdiff*) traveltime data collected by the International Seismological Centre (ISC) and suggested the velocity in the lowermost 150 km of the outer core is significantly lower than that in PREM and that the gradient is nearly flat (zero). *Song and Helmberger* [1992] suggested a smaller velocity gradient about 400 km above the ICB than PREM by fitting the amplitude of long-period PKP phases recorded at WWSSN stations. Recently, the largest ever data set of PKP waveforms was assembled and the authors found that AK135 provided the best overall fit to the observations [*Garcia et al.*, 2006].

[6] But not all seismic studies support a relatively low velocity gradient at the base of the outer core. *Choy and Cormier* [1983] found that KOR5 predicts too large PKP_{Cdiff} amplitudes compared to the observations and ruled out the low velocity gradient zone above the ICB, which is consistent with their previous results [*Rial and Cormier*, 1980; *Cormier*, 1981]. Both *Huang* [1996] and *Kaneshima et al.* [1994] investigated the ICB velocity structure beneath North America's Pacific seashore and they obtained a slightly smaller P wave velocity than that in PREM, but significantly larger than that in AK135 at the base of the outer core. Most recently *Yu et al.* [2005] re-examined the outer core velocity structure by analyzing differential traveltimes, amplitude ratios and waveforms of various *PKP* waves recorded at Global Seismograph Network (GSN) and several regional networks and they found out that the velocity structure at the base of the outer core exhibited a strong hemispherical difference. The data sampling the quasi-eastern hemisphere (40°W–180°E) can be explained by a PREM-type outer core velocity structure, while those sampling the quasi-western hemisphere (180°W–40°E) can be best explained by their preferred model OW, which has velocity closer to PREM2 than PREM at the base of the outer core.

[7] In this study, we focus on studying the structure of the base of the outer core by analyzing PKP_{Cdiff} waves, which are waves diffracted around the ICB and are more sensitive to the base of the outer core than any other phase. Although ray theory predicts zero amplitude after the C-cusp (Figure 2), which occurs at a distance of ~152.5° in PREM or ~155.5° in AK135 for a source at 100 km depth, both theoretical calculations [*Cormier and Richards*, 1977; *Cormier*, 1981] and observations [*Huang*, 1996] indicate that PKP_{Cdiff} has significant energy for several degrees into the inner core shadow zone. At these distances the amplitude decay of PKP_{Cdiff} is mainly controlled by diffraction and is extremely sensitive to the velocity gradient just above the ICB and the period of PKP_{Cdiff}.

[8] Systematic study of PKP_{Cdiff} at distances greater than 154° has been somewhat neglected because it is difficult to observe. Small earthquakes do not generate PKP_{Cdiff} waves large enough to be observed above the background noise, and large earthquakes usually have long source durations, which makes PKP_{DF} interfere with PKP_{Cdiff} (the time separation between them is less than 10 s). Similarly, shallow earthquakes sometimes generate PKP_{DF} depth phases that interfere with PKP_{Cdiff}, though with careful modeling of the source time functions this problem can often be overcome.

[9] The proliferation of regional broadband arrays over the last decade has made the observations of PKP_{Cdiff} waves less difficult, and has enabled us to assemble a large, high-quality set of PKP_{Cdiff} waveforms. In order to reduce shallow structure effects, we use PKP_{DF} as a reference phase since it has a raypath very similar to PKP_{Cdiff} in the crust and mantle. Although the top of the inner core always has an effect on the traveltime and amplitude of PKP_{DF}, our synthetic tests show that this effect is small compared with the effect of the base of the outer core on PKP_{Cdiff}. Therefore the differential traveltimes and amplitude ratios between PKP_{DF} and PKP_{Cdiff} measured from the high-quality record sections provide an excellent opportunity to explore the structure at the base of the outer core.

2. Assembly of PKP_{Cdiff} Waveform Database

[10] Because PKP_{Cdiff} is only observable over a very limited range of source-receiver distances and has relatively small amplitude, a closely-spaced seismic array is important to identify the phase and to generate a high-quality PKP_{Cdiff} data set. An array allows small coherent phases to be identified and isolated, and slowness estimates can be made to verify the identity of prospective phases. Another advantage is that the differential traveltimes (PKP_{Cdiff}–PKP_{DF}) can be measured more accurately by cross-correlating waveforms in the PKP_{Cdiff} time window and the PKP_{DF} time window respectively, instead of cross-correlating the PKP_{Cdiff} window with the PKP_{DF} window for a single station. This is especially important because diffracted waves undergo some shape change as they arrive at larger distances, and so they have shapes dissimilar with PKP_{DF}.

[11] We systematically examined the waveforms of earthquakes with depth greater than 60 km and magnitude greater than 5.5 M_w from all the temporary PASSCAL

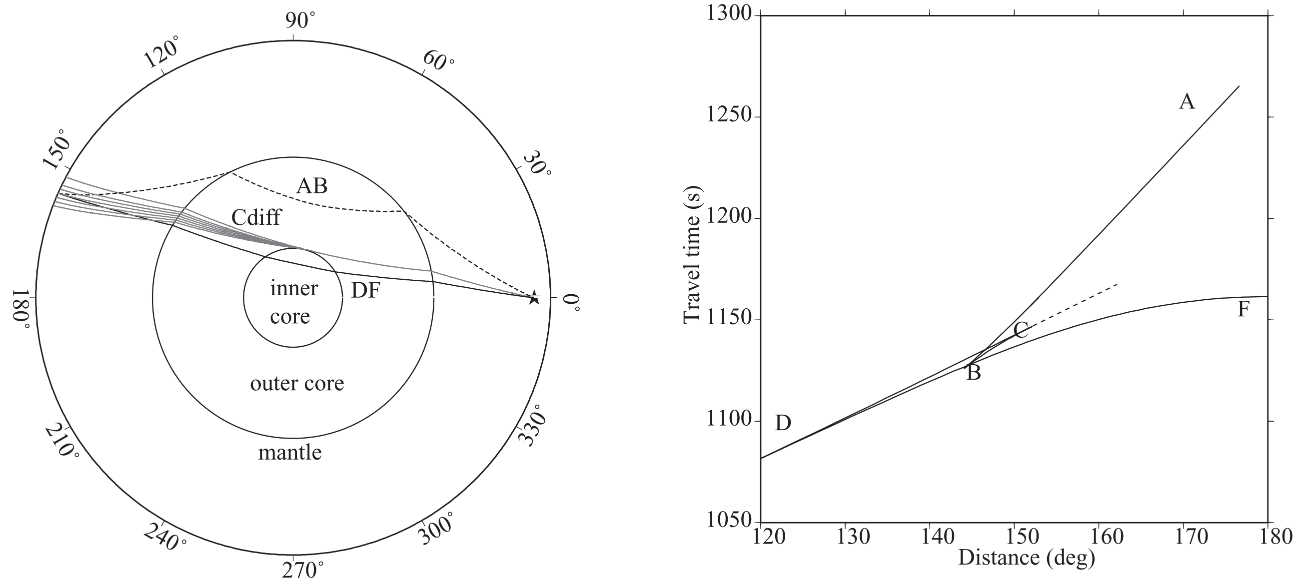

Figure 2. (Left) Raypath for *PKP* waves at the C-cusp for an event at 400 km depth. Black curve represents the raypath of PKP_{DF} at a distance of 156°. Gray curves indicate the raypaths of *PKP* waves diffracted along the ICB. (Right) Standard traveltime curve for *PKP* waves in PREM. The dashed line indicates propagation of PKP_{Cdiff}.

networks with data open to public researchers at the IRIS DMC, as well as some permanent regional seismic arrays such as F-NET (Full Range Seismograph Network of Japan) and GRF (Gräfenberg) array in Germany. Deep earthquakes have relatively short source durations, which enables us to separate PKP_{DF} and PKP_{Cdiff} more easily since the differential time between these two phases is about 10 s. Also, deep sources avoid the potential interference of the depth phase $pPKP_{DF}$ with PKP_{Cdiff}.

[12] All the record sections in the distance range 154°–160° were checked by eye for quality. We picked those events that have high signal-to-noise ratios (SNRs) records and show clear PKP_{DF} and PKP_{Cdiff} phases (Figure 3). The amplitudes of PKP_{Cdiff} waves decay with distance and are almost at the noise level after a few degrees. In our data selection criteria, we choose all the traces with high SNRs after 154° until the one at which the PKP_{Cdiff} phase is no longer identifiable. We discuss the possible bias caused by choosing only the "best" data in a later section of this manuscript.

[13] As expected, the PKP_{Cdiff} waves are very difficult to observe. We examined 111 record sections from F-net, 110 record sections from GRF, and more than 300 record sections from the temporary networks at IRIS DMC in the distance range 154°–160°. The total number of seismograms inspected was about 11,000. We obtained only 21 record sections, corresponding to 370 individual seismograms, which show high-quality PKP_{Cdiff} waves. Table 1 lists all the events and the corresponding seismic arrays used in this study. Among the 21 events in Table 1, 10 events were recorded at F-NET, 3 events were recorded at GRF, 2 events were recorded by the BANJO/SEDA (Broadband Andean Joint and Seismic Exploration of the Deep Altiplano) experiment, 2 events were recorded from INDEPTH-II (International Deep Profiling of Tibet and Himalayas, Phase II) experiment and 4 events were recorded by the INDEPTH-III experiment. Because of the small number of high quality seismograms, the geographical sampling of the core by the PKP_{Cdiff} data set is limited (Figure 4). Most of our data sample the quasi-western hemisphere (180°W–40°E) with limited sampling points in the quasi-eastern hemisphere (40°E–180°E).

3. Analysis of Differential Traveltimes ($PKP_{Cdiff}-PKP_{DF}$)

3.1. Data Processing

[14] Differential PKP_{Cdiff}–PKP_{DF} traveltimes from our data set are measured as follows. First for each record section, we filter velocity seismograms with a 3-pole Butterworth bandpass filter around 3 s with a one octave band. Although in theory filtering the seismograms at different frequency bands can provide us a separate constraint about the velocity structure at the base of the outer core, unfortunately, we found that it is difficult to get accurate measurements of PKP_{Cdiff}–PKP_{DF} traveltimes at higher or lower frequencies. At longer periods, the short time interval between PKP_{DF} and PKP_{Cdiff} makes them interfere with each other [*Souriau and Roudil*, 1995]. At higher frequencies, noise and complicated waveforms prohibit cross-correlation from working properly to get accurate traveltime estimates. Around 3 s, PKP_{Cdiff} and PKP_{DF} are well separated, and we can obtain the most accurate measurements for the differential times and the amplitude ratios.

[15] After filtering, we use the multichannel cross-correlation method (mccc) [*van Decar and Crosson*, 1990] to align the record section within the PKP_{DF} time window to get relative time shifts. Then we stack the aligned record section to get the time of the peak amplitude. By using those relative time shifts and the time of the peak amplitude, we can get the arrival times of PKP_{DF} as described by *van Decar and Crosson* [1990]. Repeating the same procedure

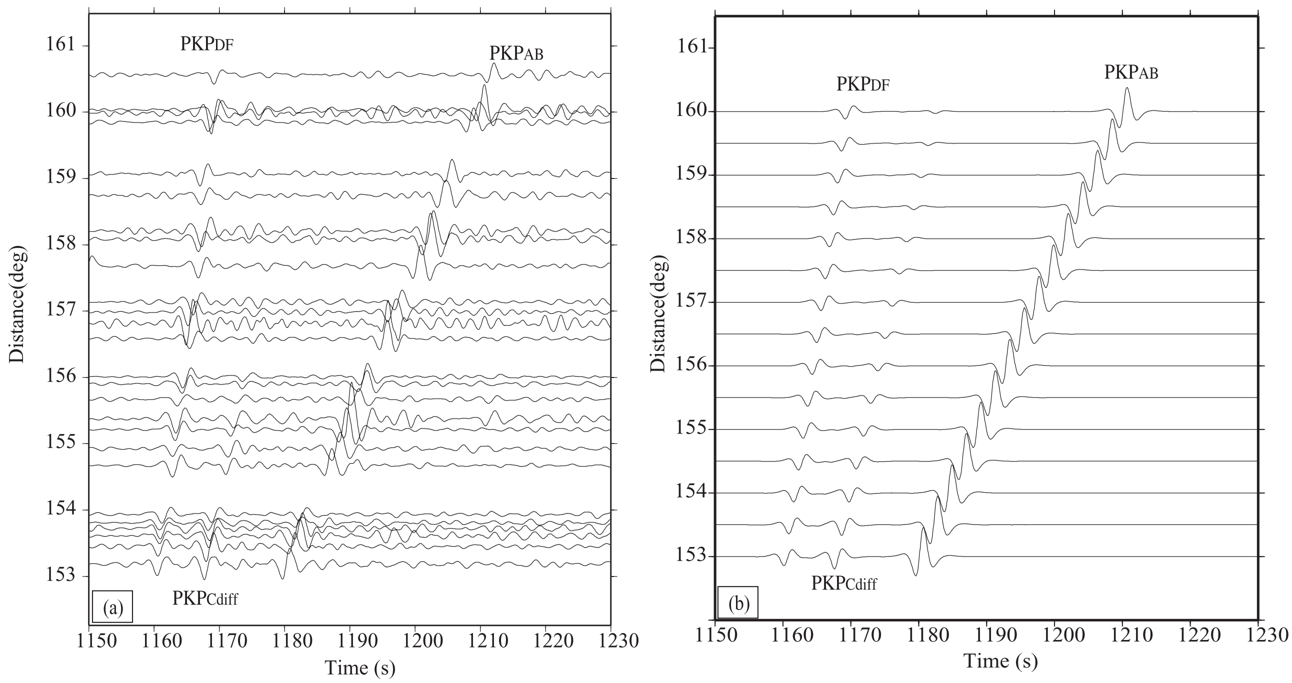

Figure 3. (a) An example of vertical seismic record sections which show good PKP_{DF} and PKP_{Cdiff} waveforms from an event recorded at F-net array with magnitude 6.1 Mw and depth 274 km (Event No. 4 in Table 1). Seismograms are filtered around 3-s using band-pass filtering. (b) The corresponding synthetic seismograms computed from full-wave theory method for an explosive source at depth of 274 km based on PREM model.

for PKP_{Cdiff}, we get the traveltime of PKP_{Cdiff} and then the differential times PKP_{Cdiff}–PKP_{DF}. The differential times measured by the mccc method were compared with those obtained with the adaptive stacking technique [*Rawlinson and Kennett*, 2004], which was proposed specifically for aligning waveforms with somewhat dissimilar shapes. The methods give almost identical results for the PKP_{Cdiff}–PKP_{DF} differential times. For each record section, we also invert the arrival times yielded by mccc for the slowness and back azimuth of PKP_{DF} and PKP_{Cdiff} phases. We find that they are generally very close to the predicted values in AK135 for most of the events, which ensures that we are indeed analyzing the proper phases. For a few events the deviations are somewhat big, but in these cases the standard

Table 1. Events and Seismic Arrays Used in This Study

Event ID	Event Time, yr/mon/day/hr:min	Lat, °N	Lon, °E	Depth, km	Mag, Mw	Array[a] Code	#[b] and, deg	ϕ[c]
1	1997/07/20/10:14	−22.98	−66.30	256	6.1	FN	12	60
2	1999/11/21/03:51	−21.75	−68.78	101	5.8	FN	8	62
3	2000/06/16/07:55	−33.88	−70.09	120	6.4	FN	22	54
4	2001/06/29/18:35	−19.52	−66.25	274	6.1	FN	23	62
5	2002/09/24/03:57	−31.52	−69.20	119	6.2	FN	32	55
6	2003/09/17/21:34	−21.47	−68.32	127	5.7	FN	14	62
7	2004/09/11/21:52	−57.98	−25.34	64	6.1	FN	24	43
8	2005/06/12/19:26	−56.28	−26.98	95	6.0	FN	26	44
9	2005/06/13/22:44	−19.90	−69.13	111	7.7	FN	26	63
10	2005/08/14/02:39	−19.74	−69.02	83	5.8	FN	12	63
11	1994/06/16/18:41	−15.18	−70.34	225	5.9	DII	9	67
12	1994/08/19/10:02	−26.65	−63.38	565	6.4	DII	8	61
13	1994/09/28/17:33	−5.72	110.38	634	6.0	BS	18	83
14	1994/11/15/20:18	−5.61	110.20	559	6.5	BS	14	83
15	1998/10/08/04:51	−16.12	−71.40	136	6.1	DIII	27	66
16	1999/03/02/17:45	−22.72	−68.50	110	5.9	DIII	27	62
17	1999/03/05/00:33	−20.42	−68.90	110	5.8	DIII	27	63
18	1999/04/03/06:17	−16.66	−72.66	87	6.8	DIII	30	64
19	1995/10/14/08:00	−25.57	−177.51	70	6.2	GRF	13	52
20	1997/04/12/09:21	−28.17	−178.37	184	5.9	GRF	13	51
21	2001/03/11/00:50	−25.37	−177.97	231	5.8	GRF	13	53

[a]For the array code, FN stands for F-net, DII stands for INDEPTH-II, DIII stands for INDEPTH-III, BS stands for BANJO/SEDA, and GRF stands for Gr*ä*fenberg.
[b]# is the number of seismograms used in the record section.
[c]ϕ is the angle of the turning direction of PKP_{DF} in the inner core with respect to the Earth's rotation axis.

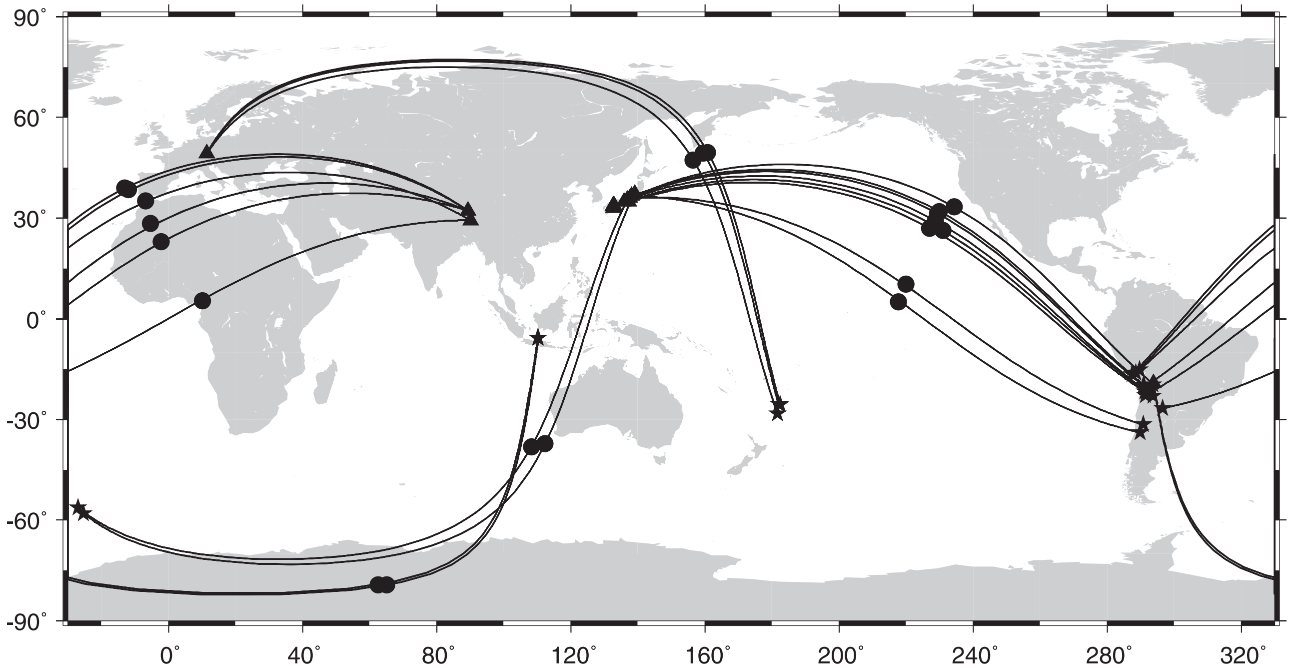

Figure 4. The great circle paths from earthquakes to corresponding seismic arrays for high-quality PKP_{DF} and PKP_{Cdiff} waveforms. The triangles are seismic arrays, the stars are earthquake locations, and the black circles indicate the turning point of PKP_{DF} in the inner core.

errors are also large because of poor source-receiver geometry. As an example, we have poor backazimuth resolution for some events recorded at INDEPTH-III because the strike of the array matches the expected backazimuth [see *Zou et al.*, 2007, Figure 1].

[16] We apply this same method to predict PKP_{Cdiff}–PKP_{DF} differential times for arbitrary velocity models using synthetic seismograms calculated with the full-wave theory technique [*Cormier and Richards*, 1977]. This method works with spherically symmetric, anelastic Earth models parametrized as polynomial functions of normalized radius. Full-wave theory correctly accounts for the diffraction and tunneling of body waves at and near the grazing incidence to a boundary by incorporating the Langer approximation [*Cormier and Richards*, 1988]. This technique is computationally fast and because it operates in spherical geometry it avoids the earth-flattening approximation. It has shown good agreement with the reflectivity method [*Choy et al.*, 1980] and the generalized ray method [*Song and Helmberger*, 1992] for generating synthetic core phases. An example record section is shown in Figure 3. We compared full wave theory synthetics to those calculated using a frequency-wave number (fk) integration method [*Zhu and Rivera*, 2002; *Herrmann and Mandal*, 1986] and found slightly different results; however, the fk synthetics contained some artifacts that were presumably related to layering in a flattened Earth model.

[17] Our observed PKP_{Cdiff}–PKP_{DF} differential traveltimes are plotted relative to PREM in Figure 5. The effect of different source depth is accounted for as follows. For each event's depth and distance, we find the PKP_{DF} ray parameter predicted by PREM. For that ray parameter, we find the corresponding distance for an event at 100 km depth, which is the distance plotted in Figure 5. All the synthetics are computed with a source depth at 100 km. Although the data are somewhat scattered, it appears that AK135 fits the data better than PREM. We use a statistical method called an *F* test [*Menke*, 1989] to verify this quantitatively. First, we calculate the variances of the misfits between the data and the predicted values from the two models, which are 0.1524 for AK135 and 0.2117 for PREM, respectively. The *F* value is then formed from the ratio of the two variances, which is 1.3891. Using an *F*-calculator (http://faculty.vassar.edu/lowry/tabs.html), we find that there is only a 0.16% probability that the two models are equal, which implies that AK135 is better than PREM at a 99.8% probability in terms of fitting the data. However, we do not observe obvious quasi-hemispherical differences in the data as seen for instance by *Yu and Wen* [2006]. Although the average differential traveltime residual for the eastern hemisphere (crosses in Figure 5) is a little bigger than for the western hemisphere (gray dots in Figure 5), the scattering ranges of the data overlap. The reason for the lack of a clear hemispherical signal may be that our data set is limited in the eastern hemisphere, or because the hemispherical pattern of the inner core velocity observed by some studies [*Niu and Wen*, 2001; *Wen and Niu*, 2002; *Garcia*, 2002; *Stroujkova and Cormier*, 2004; *Yu et al.*, 2005; *Yu and Wen*, 2006] disappears at larger distances (such as the range considered here) as reported by other authors [*Garcia et al.*, 2006; *Garcia*, 2002; *Cao and Romanowicz*, 2004]. This would be expected if the quasi-hemispherical pattern in the inner core exists only to relatively shallow depths beneath the ICB.

3.2. Data Modeling

[18] In modeling the traveltime data we only vary the velocity structure at the base of the outer core and fix the

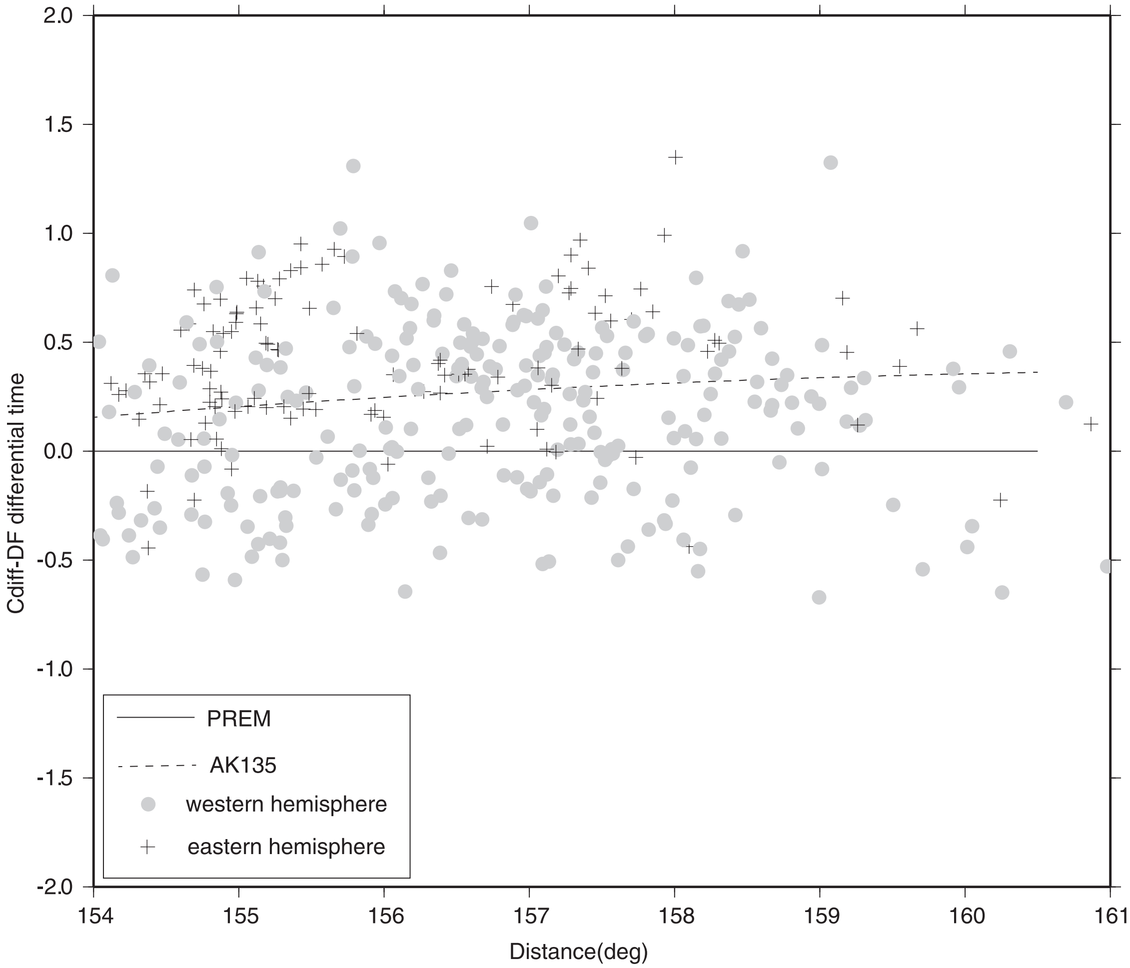

Figure 5. Observed $PKP_{Cdiff} - PKP_{DF}$ differential traveltimes relative to PREM. The solid line is for PREM, which is zero since it is used as a reference. The dashed line represents predicted differential times of AK135 relative PREM. The pluses are for the data sampling the eastern hemisphere, and the gray circles are for the data sampling the western hemisphere.

velocity in the remainder of the Earth according to PREM. There are several reasons why this type of limited parametrization is justified. First, because the raypaths of PKP_{DF} and PKP_{Cdiff} are very close in the crust and most of the mantle, the differential times can be attributed mainly to the velocity structure in the lower outer core and at most the upper 500 km of the inner core. For our distance range of 154°–160° the reference phase PKP_{DF} turns at 300–500 km below the ICB, while PKP_{Cdiff} has maximum sensitivity just above the ICB. Second, the difference in inner core and the lowermost mantle velocity structure between standard reference models has very small effects on PKP_{Cdiff}–PKP_{DF} differential times, while the difference in the velocity at the base of outer core between standard reference models has a large effect (Figure 6). Third, we note that the angle of PKP_{DF} with respect to Earth's rotation axis for all our data is greater than 45° (Table 1). On the basis of the reported inner core anisotropy models [e.g., *Creager*, 1992; *Shearer*, 1994; *Vinnik et al.*, 1994; *Song and Richards*, 1996], the traveltime difference of PKP_{DF} caused by anisotropy is very small (less than 0.2 s). So the observed differential times PKP_{Cdiff}–PKP_{DF} would not be affected significantly by inner core anisotropy. Fourth, we do not observe a strong quasi-hemispherical signal in the data, and so separate modeling for each hemisphere is not warranted.

[19] Among velocity models at the base of the outer core reported by different studies [e.g., *Qamar*, 1973; *Dziewonski and Anderson*, 1981; *Choy and Cormier*, 1983; *Souriau and Poupinet*, 1991; *Song and Helmberger*, 1995; *Kennett et al.*, 1995; *Yu et al.*, 2005], the main difference is the structure of the velocity and its gradient at the bottom 400 km (or less) of the outer core. In PREM [*Dziewonski and Anderson*, 1981], the velocity increases with a nearly constant gradient around 0.6×10^{-3} s^{-1}. In PREM2 [*Song and Helmberger*, 1995] and AK135 [*Kennett et al.*, 1995], the velocity gradient decreases from about 0.6×10^{-3} s^{-1} at 400 km above the ICB to nearly zero at the ICB, and the velocity profile with depth is more flat than that in PREM. Therefore we choose 400 km above the ICB as the minimum "pinning depth" at which the models we evaluate are constrained to agree with PREM in value and gradient.

[20] We use a systematic grid search to find a model that best fits the data. We let the pinning depth start at 400 km above the ICB and increase it in 50 km intervals until it is 50 km above the ICB. For each pinning depth, we keep the velocity and its gradient the same as in PREM, and let the

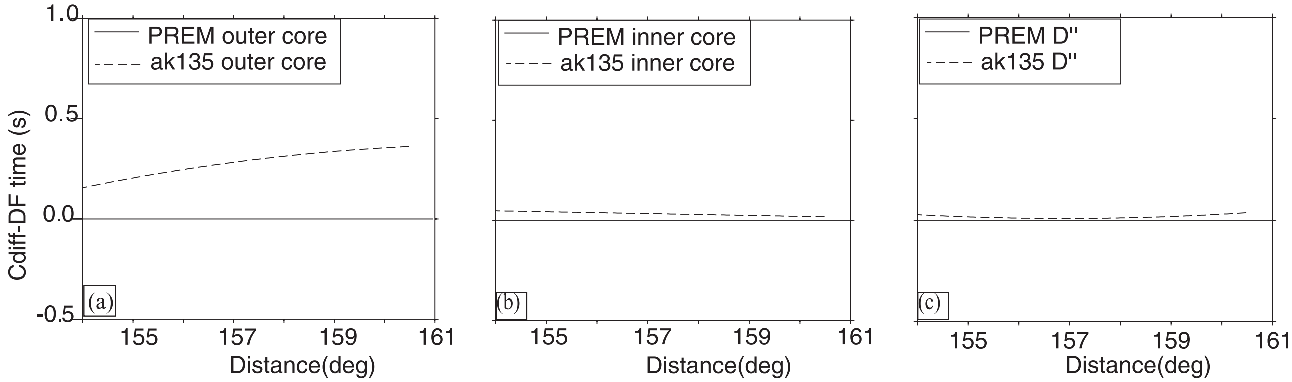

Figure 6. (a) The difference in the differential times caused by the velocity difference at the base of the outer core between PREM and AK135. (b) The difference in the differential times caused by the velocity difference in the inner core between PREM and AK135. (c) The difference in the differential times caused by the velocity difference in the lowermost mantle. In all three panels, the solid line is for PREM, and the dashed line is for AK135.

gradient decrease linearly with different slopes to satisfy the velocity gradient at the ICB between 0.6×10^{-3} s^{-1} (the value in PREM) and zero (the value in AK135) with an increment of 0.01×10^{-3} s^{-1}. We use 2nd-order polynomials (3 polynomial coefficients) to describe the velocity structure and have two constraints at the pinning depth and one constraint at the ICB. Therefore we have exact analytical solutions for the polynomial coefficients. In this way, we generate 488 different velocity models at the base of the outer core (8 different pinning depth $\times$ 61 different slopes of the gradient for each different pinning depth).

[21] For each trial velocity model, we compute the synthetic seismograms and get the PKP_{Cdiff}–PKP_{DF} differential times with the method described above. Using an L2

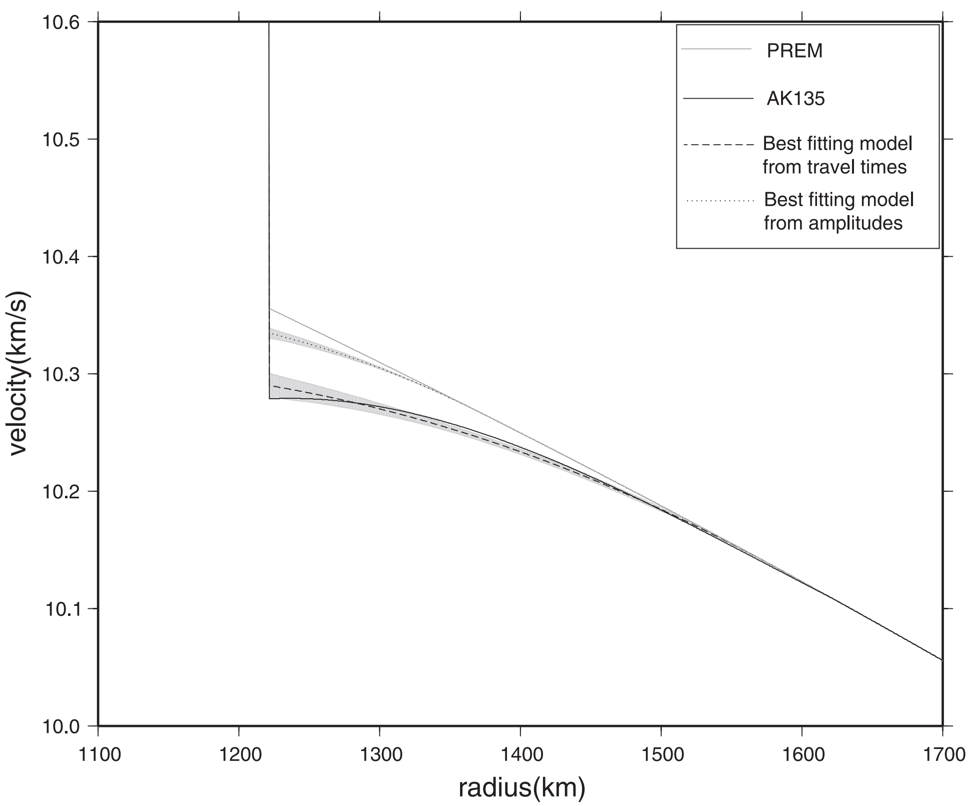

Figure 7. The best fitting model from the differential times (PKP_{Cdiff}–PKP_{DF}) and from the amplitude ratios (PKP_{Cdiff}/PKP_{DF}). The top gray curve is for PREM, the bottom black curve is for AK135, the black dashed curve with gray shaded region is the best fitting model with one standard deviation from the differential times, and the dotted black curve with gray shaded region is our best fitting model with one standard deviation from the amplitude ratios with inner core Q = 400 discussed in section 4.2.

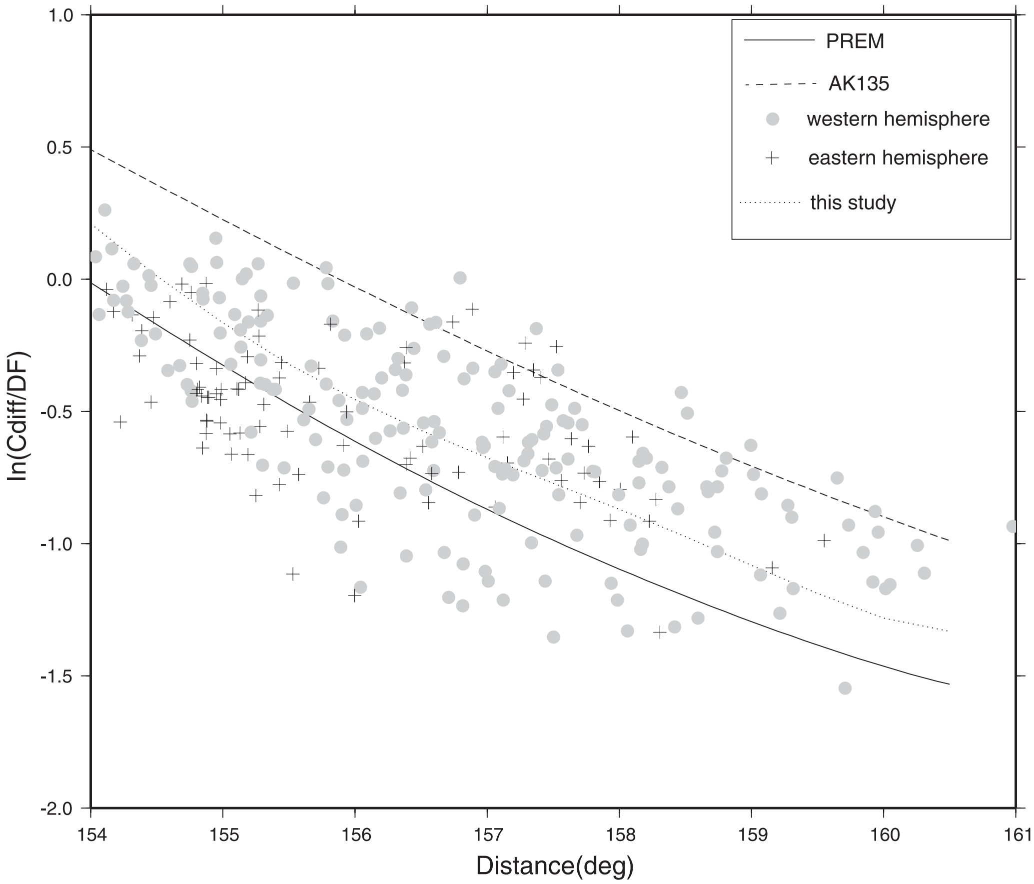

Figure 8. Observed amplitude ratios of (PKP_{Cdiff}/PKP_{DF}). The solid curve is the predicted amplitude ratios from PREM and the dashed curve is for AK135. The pluses are for the data sampling the eastern hemisphere, and the gray circles are for the data sampling the western hemisphere. The dotted curve is the synthetic amplitude ratio from the velocity model yielded by the amplitude ratios when inner core Q = 400 as shown in dotted curve in Figure 7. Both data and synthetics have been obtained from seismograms filtered with a narrow bandpass centered at 3 s.

norm misfit function between the synthetics and the data, we find a best fitting model that is very close to AK135 (Figure 7). This is consistent with the results of *Garcia et al.* [2006] who worked with a much larger data set of *PKP* arrivals at different distances. The uncertainty of our results is estimated using a bootstrap resampling algorithm [*Tichelaar and Ruff*, 1989], which randomly resamples the data with replacement to generate a pseudo-data set with the same number of elements as the true data set. An optimal solution is obtained by fitting the pseudo-data set. By repeating the procedure 200 times, we obtain a population of best fitting models and therefore the mean and standard deviation can be estimated (Figure 7).

4. Analysis of Amplitude Ratios (PKP_{Cdiff}/PKP_{DF})

[22] PKP_{Cdiff} amplitudes are very sensitive to the velocity gradient at the bottom of the outer core, just as P_{diff} amplitudes are very sensitive to the gradient at the base of the mantle [*Alexander and Phinney*, 1966; *Phinney and Alexander*, 1966; *Valenzuela and Wysession*, 1998]. Different velocity gradients focus or defocus the seismic energy in different ways. A larger positive gradient bends energy back toward the surface, causing smaller amplitudes of the diffracted waves; a negative or smaller positive gradient traps more energy near the ICB, thus causing larger amplitude of the diffracted wave into the shadow zone.

4.1. Data Processing

[23] Similar to the traveltime analyses, in order to mitigate the effects of shallow structure on PKP_{Cdiff} amplitude, we use the amplitude ratios between PKP_{Cdiff} and PKP_{DF} to constrain the velocity structure at the base of the outer core. The procedure we use to obtain the amplitude ratios is similar to the one used to get the differential times. We measure the peak-to-peak amplitudes from the filtered seismograms for both PKP_{DF} and PKP_{Cdiff}. Synthetic amplitude ratios are obtained in the same way from the synthetic seismograms computed with full-wave theory for an explosive source. In order to compare the observed amplitude ratios with the synthetic ones, we apply the source corrections to the data by using radiation coefficients of PKP_{DF} and PKP_{Cdiff} according to the Harvard CMT focal mechanism. Since the take-off angles of PKP_{DF} and PKP_{Cdiff} are very close, the corrections are quite small. The distance of each measurement is adjusted for focal depth using the same approach as in the traveltime analysis. The corrected measurements are presented in Figure 8. The

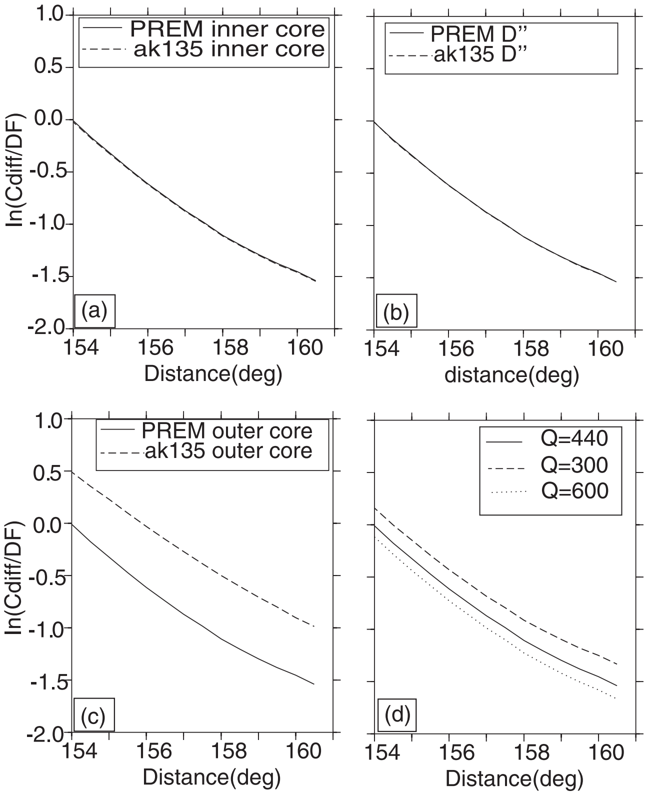

Figure 9. (a) The difference in the amplitude ratios (PKP_{Cdiff}/PKP_{DF}) caused by the velocity difference in the inner core between PREM and AK135. (b) The difference in the amplitude ratios (PKP_{Cdiff}/PKP_{DF}) caused by the velocity difference in the lowermost mantle between PREM and AK135. (c) The difference in the amplitude ratios caused by the velocity difference at the base of the outer core between PREM and AK135. In panel (a), (b) and (c), the solid curve is for PREM and the dashed one is for AK135. (d) The difference in the amplitude ratios caused by different inner Q values. The solid curve is for Q = 440, the dashed one is for Q = 300 and the dotted one is for Q = 600.

observed amplitude ratios do not exhibit clear hemispherical differences, which is consistent with the amplitude observations of [*Yu and Wen*, 2006] (see their Figure 5), as well as the traveltime observations presented here (Figure 5). However, the amplitude ratios observed by [*Souriau and Roudil*, 1995] (see their Figure 8) are consistently larger than our data. They also filtered the seismograms around 3 s to get the measurements, and so the differences must be due to different Earth sampling or data quality. One possibility for the discrepancy is that by using arrays to identify PKP_{Cdiff} waves we are able to confidently include smaller phases, while the data set of [*Souriau and Roudil*, 1995] only includes phases that were large enough to be confidently identified on individual seismograms.

4.2. Data Modeling

[24] Before we evaluate the different trial models, we perform sensitivity tests to see what Earth properties most affect PKP_{Cdiff}/PKP_{DF} amplitude ratios. As expected, we find that the difference in the inner core and the lowermost mantle velocity between different reference models does not affect the amplitude ratios significantly, but that the difference in the velocity at the base of the outer core has a very prominent effect on the amplitude ratios (Figure 9). A smaller velocity gradient at the bottom of the outer core tends to generate larger PKP_{Cdiff} amplitudes, thus larger amplitude ratios (PKP_{Cdiff}/PKP_{DF}). Therefore AK135 predicts much larger PKP_{Cdiff}/PKP_{DF} amplitude ratios than PREM. We also confirmed that the difference in the velocity at the base of the outer core between PREM and AK135 has nearly no effect on the PKP_{DF} amplitude. Thus the large amplitude ratios from AK135 are totally due to the large PKP_{Cdiff} amplitudes. Unlike the differential traveltimes, however, the effect of inner core P wave attenuation (Q) on amplitude ratios is not negligible (Figure 9c). Smaller Q in the inner core decreases the PKP_{DF} amplitude, and thus increases the PKP_{Cdiff}/PKP_{DF} amplitude ratio. Therefore there is always a trade-off between inner core attenuation and the velocity structure at the base of the outer core.

[25] We perform a similar grid search over the velocity structure at the base of the outer core as we did for the traveltimes. To account for the effects of inner core attenuation, we assign different inner core Q values (300, 400, 500, 600) for each of the velocity models. This range is defined based on the results of several recent investigations [e.g., *Dziewonski and Anderson*, 1981; *Bhattacharyya et al.*, 1992; *Wen and Niu*, 2002; *Cao and Romanowicz*, 2004; *Yu and Wen*, 2006; *Garcia et al.*, 2006]. Therefore the total number of models we evaluate is four times those evaluated in the traveltime analysis. By minimizing the L2-norm misfit function between the observed and synthetic amplitude ratios in log-space, we find the best fitting model.

[26] Not surprisingly, for different values of inner core Q, we obtain different best fitting models. However, all the models are significantly different from the best model found by fitting the traveltimes. Even when we let the inner core Q be 600, the best model with respect to the amplitude ratios still has significantly faster velocity at the base of the outer core than the best model with respect to the differential times. For example, the dotted line with shadowed area in Figure 7 shows the best fitting model and its uncertainty obtained from bootstrap resampling algorithm with a reasonable inner core Q value of 400. The corresponding predicted amplitude ratio curve is presented in Figure 8 as the dotted curve. A smaller inner core Q value decreases the PKP_{DF} amplitude, and thus requires a smaller PKP_{Cdiff} amplitude, which corresponds to a steeper velocity structure. The best model from the traveltimes gives too big PKP_{Cdiff} amplitudes that are inconsistent with our observations.

[27] We check the robustness of this result with several additional tests. Allowing for a depth-dependent inner core Q, by using different combinations of Q in the upper 200 km of the inner core (Q from 100 to 1000) and Q for the rest of the inner core (Q from 600 to 1000), we find PKP_{Cdiff}/PKP_{DF} amplitude ratios for the best traveltime derived velocity model are consistently too large compared to the observations. We find the same result for several other high-quality velocity models determined in section 3.2. Considering a frequency-dependent inner core Q model suggested previously [e.g., *Li and Cormier*, 2002; *Cormier and Li*, 2002], we experiment with lower corner frequency of 0.1–0.5 Hz and find that they do not significantly change the amplitude ratios as well. We also find that changes to the

density jump and shear velocity jump across the ICB have relatively small changes on the theoretical amplitude ratios, and do not allow the traveltime data to be reconciled with the amplitude data.

5. Discussion

[28] Our PKP_{Cdiff}–PKP_{DF} differential times give a flatter velocity structure at the base of the outer core than PREM [*Dziewonski and Anderson*, 1981], which may imply a different chemical composition at the base of the outer core, as suggested by previous studies [*Souriau and Poupinet*, 1991; *Song and Helmberger*, 1995]. However, our PKP_{Cdiff}/PKP_{DF} amplitude ratios do not support this feature (Figure 7), instead they prefer a PREM-type velocity structure at the base of the outer core, regardless of inner core Q values. This apparent discrepancy is indirectly supported by many previous studies. The result from the differential times is especially consistent with those studies based on traveltimes [e.g., *Souriau and Poupinet*, 1991; *Song and Helmberger*, 1995; *Kennett et al.*, 1995; *Yu et al.*, 2005]. Meanwhile, our result from the amplitudes ratios is consistent with previous PKP_{Cdiff} amplitudes studies [*Choy and Cormier*, 1983; *Cormier*, 1981]. Note that it is also consistent with the results of PREM2 [*Song and Helmberger*, 1995]. In that study the authors found that for either constant Q or constant t^* in the inner core, the PKP_{Cdiff}/PKP_{DF} amplitude ratios predicted by PREM2 were larger than the observations [see *Song and Helmberger*, 1995, Figure 8].

[29] It is also important to point out that any potential bias in our data selection magnifies the discrepancy. By choosing only waveforms with high quality *PKP* phases, it is possible that our data set is skewed toward abnormally large PKP_{Cdiff} waves. However, the best fitting traveltime model would be inconsistent with PKP_{Cdiff} waves even larger than what we observe. In other words, if a hypothetical perfectly averaged PKP_{Cdiff} data set has lower amplitudes than our data set, the discrepancy with the traveltimes would be even bigger than what we observe.

[30] To summarize, the observed PKP_{Cdiff} amplitudes are smaller than what is expected. This is analogous to earlier seismological studies that found unexpectedly small amplitudes for P_{diff} amplitudes, suggesting some sort of complexity in the lowermost mantle [e.g., *Ruff and Helmberger*, 1982]. In that case, the preferred interpretation of the authors was of a jagged, but positive velocity gradient in the lowermost mantle, implying that D'' is more complicated than a simple, thermal boundary layer. However, in our case the velocity structure just above the ICB cannot be altered to match the observed amplitudes because the predicted traveltimes would then become inaccurate. Instead a non-standard mechanism must exist that acts to reduce PKP_{Cdiff} amplitudes while not significantly affecting the corresponding traveltimes. It appears that the small-scale heterogeneity inside the inner core observed by many authors [e.g., *Vidale and Earle*, 2000; *Cormier and Li*, 2002; *Koper et al.*, 2004; *Leyton and Koper*, 2007] would not be able to explain this discrepancy because the inner core scattering would decrease the PKP_{DF} amplitude and thus increase the PKP_{Cdiff}/PKP_{DF} ratios. We believe the two primary candidates for explaining the observed discrepancy are (1) small-scale topography or roughness on the ICB that scatters energy from the main PKP_{Cdiff} phase into trailing coda waves, and (2) a layer at the base of the outer core that possesses low intrinsic Q owing to anelastic mechanisms.

5.1. Hypothesis #1: A Rough ICB

[31] Although strong coda waves following PKP_{Cdiff} have been observed, they are generally not interpreted as being caused by irregularities at the ICB [*Nakanishi*, 1990; *Tanaka*, 2005; *Zou et al.*, 2007]. Slowness information derived from array and polarization analysis tends instead to support scatterer locations in the mantle. However, these studies do not exclude a contribution to PKP_{Cdiff} coda waves from complexities at the ICB, and several recent studies have found independent evidence favoring a rough ICB. *Poupinet and Kennett* [2004] proposed inner core boundary scattering to explain the complexity of the *PKiKP* coda recorded at Warramunga seismic array and suggested the ICB has some short-scale heterogeneities with lowered wave speed. *Koper and Dombrovskaya* [2005] found large variation in *PKiKP*/*P* amplitude ratios and suggested the presence of heterogeneities at, or very near the ICB. Significant variability of *PKiKP* amplitudes from explosion sources also led to the suggestion of a mosaic structure at the inner core's surface [*Krasnoshchekov et al.*, 2005]. Most recently, high-quality earthquake doublet data recorded at different locations suggested that small-wavelength, irregular topography is present at the ICB [*Wen*, 2006; *Cao et al.*, 2007].

[32] To evaluate this hypothesis numerical simulations of short-period PKP_{Cdiff} waves for rough ICB models need to be carried out to determine if geodynamically reasonable structures have the desired effect. This is a difficult problem that is outside the scope of this paper, but it is potentially feasible using modern computation approaches such as the axi-symmetric finite difference method that has recently been used to simulate the effect of complicated CMB models on ScS and core grazing S waves [*Lay et al.*, 2006], or the pseudo-spectral method recently applied to inner core scattered waves [*Cormier*, 2007]. A numerical evaluation is also important because of the counter-intuitive possibility that a rough ICB would lead to enhanced PKP_{Cdiff} amplitudes, as in Biot scattering associated with seafloor topography [*Menke*, 1982].

5.2. Hypothesis #2: A Slurry Zone at the Base of the Outer Core

[33] In this scenario, we hypothesize that intrinsic attenuation in the lowermost outer core is much higher compared to the rest of the outer core. Thus the amplitude of PKP_{Cdiff} would be significantly reduced while traveling horizontally in the low-Q layer, but PKP_{DF} amplitudes would be less affected because of the steeper raypaths through the layer. This type of model has been suggested on geodynamical grounds and termed a slurry zone [*Loper and Roberts*, 1978, 1981; *Loper*, 1978]. Such a feature could be formed by the nucleation and gradual precipitation of solid particles from super-cooled fluid at the base of the outer core. Alternatively, the super-cooling instability could lead to the radial growth of dendritic arms of solid material from the inner core into the outer core, forming a thin, mushy zone; presumably, dendrites from the mushy zone could be broken and distributed throughout the base of the outer core by

large scale convective motions [*Copley et al.*, 1970; *Loper and Roberts*, 1978]. Internal friction between suspended solid particles and the surrounding fluid is expected for seismic waves traversing the region, and therefore the slurry layer might be expected to have relatively low Q compared to the rest of the outer core.

[34] To our knowledge, there has been only one seismic study in which such a model has been quantitatively evaluated [*Cormier*, 1981]. In this model (designated as QIC3) Q increased smoothly from 200 to 10,000 as the radius increased from the ICB to about 250 km shallower. QIC3 was rejected because it underpredicted absolute short-period PKP_{DF} amplitudes measured at WWSSN stations [*Buchbinder*, 1971]. However, we note that QIC3 also possessed an extremely low-Q layer at the top of the inner core, with a minimum Q value of 125 just beneath the ICB tapering to a Q value of 1000 about 250 km beneath the ICB.

[35] To evaluate the possibility of a low-Q layer at the base of the outer core we carry out a systematic grid search similar to the ones described earlier. We fix the velocity structure to the model preferred by the PKP_{DF}–PKP_{Cdiff} differential traveltimes (Figure 7) and search over a range of Q values (from 100 to 600 with 50 as the interval) and thicknesses (from 50 km to 400 km with 50 km as the interval) to find the parameters that best fit the observed PKP_{DF}/PKP_{Cdiff} amplitude ratios. Assuming an inner core Q of 400, the best model has a Q of 300 over the bottom 350 km of the outer core. In this case, the predicted amplitude ratio curve is very close to the synthetic curve (the dotted curve in Figure 8) from the best model preferred by the amplitude ratios. Unfortunately, the problem is underdetermined as there are significant trade-offs among the model parameters: between inner core Q and outer core Q, and between outer core Q and layer thickness. However, we do find that extremely thin (<100 km) outer core low-Q layers are incompatible with the amplitude ratios because they lead to overly steep decay rates.

[36] The best fitting models found above significantly reduce absolute PKP_{DF} amplitudes, although not as much as QIC3. For instance, with a Q of 300 at the bottom 350 km outer core, PKP_{DF} amplitude decreases by 24%, and PKP_{Cdiff} amplitude decreases by 52% at distance of 158°. This effect would be expected to be larger at smaller distances, as PKP_{DF} travel less steeply through the base of the outer core; however, the variation in absolute PKP_{DF} amplitude is on the same order predicted for models with extremely low-Q layers at the top of the inner core and a standard outer core model.

6. Conclusions

[37] We systematically searched the high-quality PKP_{Cdiff} waveforms from all the temporary networks with data currently available at IRIS DMC and some regional seismic arrays to assemble the largest PKP_{Cdiff} data set ever. Our best model derived by fitting the differential times (PKP_{Cdiff}–PKP_{DF}) indicates that the velocity and its gradient at the base of the outer core are significantly lower than those in PREM, which is consistent with many previous studies [e.g., *Souriau and Poupinet*, 1991; *Song and Helmberger*, 1995; *Kennett et al.*, 1995; *Yu et al.*, 2005]. The relatively low gradient at the base of the outer core implies that the Bullen parameter is significantly greater than 1, which in turn implies the existence of an abnormally dense layer at the base of the outer core [*Souriau and Poupinet*, 1991; *Song and Helmberger*, 1995]. This may explain why recent body wave estimates of the density jump across the ICB are smaller than estimates made from broadly sensitive normal mode observations [*Koper and Dombrovskaya*, 2005].

[38] However, our best fitting model derived from the amplitude ratios lacks the flat velocity profile at the base of the outer core required by the traveltimes, and instead it is closer to the velocity profile in PREM. This result is also consistent with some previous PKP_{Cdiff} amplitude studies [*Choy and Cormier*, 1983; *Cormier*, 1981]. We believe the velocity profile at the base of the outer core is in fact significantly flatter than PREM, as revealed by our traveltime analysis, and that observed PKP_{Cdiff} amplitudes are reduced by a non-standard mechanism not normally included in synthetic seismograms.

[39] One way to reconcile our traveltime and amplitude observations is with the existence of rough topography on the ICB that acts to scatter energy away from PKP_{Cdiff} as it propagates horizontally above the ICB. A complicated or rough ICB has recently been suggested by several authors using independent data sets of waves reflected from the ICB [*Poupinet and Kennett*, 2004; *Koper and Dombrovskaya*, 2005; *Krasnoshchekov et al.*, 2005; *Wen*, 2006; *Cao et al.*, 2007]. This would be an elastic process in which energy is partitioned away from the main phases into later arriving coda waves. Several researchers have examined unusual looking PKP_{Cdiff} coda waves, but to date all of the analyses have preferred mantle locations for the scatterers. Nevertheless, the evidence from the *PKiKP* studies warrants the future numerical experimentation to determine if reasonable models of ICB complexity can produce the needed reduction in PKP_{Cdiff} amplitudes, while leaving PKP_{Cdiff} traveltimes relatively unchanged.

[40] A second way to reconcile our observations is with the existence of a relatively low-Q layer at the base of the outer core. For example, a model with flat velocities at the base of the outer core (similar to AK135), an inner core Q_p of 400, and a 350 km thick layer with Q_p of 300 at the bottom of the outer core fits both the traveltime and amplitude constraints. Therefore besides being unusually dense, the base of the outer core may also be unusually attenuating at body wave periods (1–10 s). A physical model for such properties was suggested by *Loper and Roberts* [1978] in the form of a slurry layer of suspended solid Fe particles in a fluid matrix. Extrapolating results of ultrasonic attenuation experiments with metal powder-viscous liquid suspensions [*Schulitz et al.*, 1998] suggests that the viscosity of such a slurry would be on the order of 10^{11} *Pa s* to produce the observed body wave attenuation. Recent metallurgical studies, however, suggest that such a slurry layer is unlikely to exist, because of the dendritic growth patterns observed in solidifying metals [*Bergman*, 1997; *Bergman et al.*, 2005]. However, a recent study (D. Gubbins, G. Masters, and F. Nimmo, A thermo-chemical boundary layer at the base of Earth's outer core and independent estimate of core heat flux, submitted to *Geophysical Journal International*, 2007) re-investigated this scenario and proposed a core model in which part of the

light components forms a solid upon freezing of the inner core, and then floats upwards and remelts at some point. To fit the seismic properties and heat fluxes, their preferred model has a 200 km thick layer at the base of the outer core which has less light elements concentration than the rest of the outer core. This provides a physical explanation for the larger density gradient and smaller velocity gradient for the bottom 200 km of the outer core, and the possible low Q there as well.

[41] Although bulk Q in the upper 1000 km of the outer core has been measured to be nearly infinity from high frequency body waves [e.g., *Cormier and Ricards*, 1976], it is possible there may be some deeper bulk attenuation. This idea of a low-Q layer at the base of the fluid core can be further evaluated in two ways. First, the optimal models reported here can be tested against the large databases of $PKP_{DF}/PKP_{AB\text{-}BC}$ amplitude ratios that exist at distances both smaller and larger than the range considered here [*Garcia et al.*, 2006]. Second, the low-Q models can be tested against normal mode observations. A recent study that used a global search algorithm to fit a large database of normal mode observations found that existing radial Q_κ models of the outer are too large by factors of 2–10 [*Resovsky et al.*, 2005]. Those authors preferred a value of $Q_\kappa \sim 6000$ for the outer core, a value much higher than suggested here for the base of the outer core; however, the outer core was treated as a single layer and no allowance was made for variation within this layer. Because the mode data averages significantly over radius, it's possible a low-Q layer is consistent with the data if a more flexible parametrization is used.

[42] **Acknowledgments.** We thank Christine Thomas and another anonymous reviewer for their insightful and constructive comments. We are grateful to the Incorporated Research Institutions for Seismology (IRIS) DMC, Full Range Seismograph Network of Japan (F-net) and Seismological Central Observatory (SZGRF) for access to the high-quality seismic data. We thank the Harvard CMT Project for making the focal mechanism information available. We used GMT [*Wessel and Smith*, 1991] to make most of the figures. This research was supported by NSF grants EAR0229586, EAR0229103, and EAR050537438.

References

Adams, R. D., and M. J. Randall (1964), The fine structure of the Earth's core, *Bull. Seismol. Soc. Am.*, *54*, 1299–1313.

Alexander, S. S., and R. Phinney (1966), A study of the core-mantle boundary using P waves diffracted by the Earth's core, *J. Geophys. Res.*, *71*, 5943–5958.

Anderson, W. W., and T. J. Ahrens (1994), An equation of state for liquid iron and implications for the Earth's core, *J. Geophys. Res.*, *99*, 4273–4284.

Bergman, M. I. (1997), Measurements of elastic anisotropy due to solidification texturing and the implications for the Earth's inner core, *Nature*, *389*, 60–63.

Bergman, M. I. (2003), Solidification of Earth's core, in *Earth's Core: Dynamics, Structure, Rotation*, *Geodyn. Ser.*, edited by V. Dehant, et al., pp. 105–127, AGU, Washington, D. C.

Bergman, M. I., M. Macleod-Silberstein, M. Haskel, B. Chandler, and N. Akpan (2005), A laboratory model for solidification of Earth's core, *Phys. Earth Planet. Inter.*, *153*, 150–164.

Bhattacharyya, J., P. Shearer, and G. Masters (1992), Inner core attenuation from short-period *PKP* (*BC*) versus *PKP* (*DF*), *J. Geophys. Res.*, *97*, 6573–6586.

Bolt, B. A. (1962), Gutenberg's early *PKP* observations, *Nature*, *196*, 122–124.

Bolt, B. A. (1964), The velocity of seismic waves near the Earth's center, *Bull. Seismol. Soc. Am.*, *54*, 191–208.

Buchbinder, G. G. R. (1971), Velocity structure of the Earth's core, *Bull. Seismol. Soc. Am.*, *61*, 429–456.

Bullen, K. E. (1963), An index of degree of chemical inhomogeneity in the Earth, *Geophys. J. Int.*, *7*, 584–592.

Cao, A., and B. Romanowicz (2004), Hemispherical transition of seismic attenuation at the top of the Earth's inner core, *Earth Planet. Sci. Lett.*, *228*, 243–253.

Cao, A., W. Masson, and B. Romanowicz (2007), Short wavelength topography on the inner-core boundary, *PNAS*, *104*, 31–35, doi:10.1073/pnas.0609810104.

Choy, G. L., and V. F. Cormier (1983), The structure of the inner core inferred from short-period and broadband GDSN data, *Geophys. J. R. Astron. Soc.*, *72*, 1–21.

Choy, G. L., V. F. Cormier, R. Kind, G. Muller, and P. G. Richards (1980), A comparison of synthetic seismograms of core phases generate by the full wave theory and by the reflectivity method, *Geophys. J. R. Astron. Soc.*, *61*, 21–39.

Cleary, J. R., and R. A. W. Haddon (1972), Seismic wave scattering near the CMB: A new interpretation of precursors to *PKP*, *Nature*, *240*, 549–551.

Copley, S., A. Giamei, S. Johson, and M. Hornbecker (1970), The origin of freckles in unidirectionally solidified casting, *Metall. Trans. A and B*, *1*, 2193–2204.

Cormier, V. F. (1981), Short-period *PKP* phases and the anelastic mechanism of the inner core, *Phys. Earth Planet. Inter.*, *24*, 291–301.

Cormier, V. F. (2007), Texture of the uppermost inner core from forward- and back-scattered seismic waves, *Earth Planet. Sci. Lett.*, doi:10.1016/j_enh.epsl.2007.04.003.

Cormier, V. F., and X. Li (2002), Frequency dependent attenuation in the inner core: Part II. A scattering and fabric interpretation, *J. Geophys. Res.*, *107*(B12), 2362, doi:10.1029/2002JB001796.

Cormier, V., and P. Ricards (1976), Comments on "The Damping of Core Waves" by Anthony Qamar and Alfredo Eisenberg, *J. Geophys. Res.*, *81*, 3066–3068.

Cormier, V. F., and P. Richards (1977), Full wave theory applied to a discontinuous velocity increase: The inner core boundary, *J. Geophys. Res.*, *43*, 3–31.

Cormier, V. F., and P. Richards (1988), Spectral synthesis of body waves in earth models specified by vertically varying layers, in *Seismological Algorithms, Computational Methods and Computer Programs*, edited by D. J. Dornboos, pp. 3–45, Academic Press, London and New York.

Creager, K. (1992), Anisotropy of the inner core from differential travel times of the phases *PKP* and *PKIKP*, *Nature*, *356*, 309–314.

Doornbos, D. J., and E. S. Husebye (1972), Array analysis of *PKP* phases and their precursors, *Phys. Earth Planet. Inter.*, *5*, 387–399.

Dziewonski, A. M., and D. L. Anderson (1981), Preliminary reference Earth model, *Phys. Earth Planet. Inter.*, *25*, 297–356.

Garcia, R. (2002), Constraints on upper inner core structure from waveform inversion of core phases, *Geophys. J. Int.*, *150*, 651–664.

Garcia, R., H. Tkalčić, and S. Chevrot (2006), A new global *PKP* data set to study Earth's core and deep mantle, *Phys. Earth Planet. Inter.*, doi:10.1016/j.pepi.2006.05.003.

Haddon, R. A. W., and J. R. Cleary (1974), Evidence for scattering of seismic *PKP* waves near the core-mantle boundary, *Phys. Earth Planet. Inter.*, *8*, 211–234.

Herrmann, R. B., and B. Mandal (1986), A study of wavenumber integration techniques, *Earthquakes Notes*, *57*, 33–40.

Huang, B. S. (1996), Investigation of the inner-outer core boundary structure from the seismograms of a deep earthquake recorded by a regional seismic array, *Geophys. Res. Lett.*, *23*, 209–212.

Jeffreys, H. (1939), The times of the core waves, *Mon. Not. R. Astron. Soc. Geophys. Suppl.*, *4*, 498.

Kaneshima, S., K. Hirahara, T. Ohtaki, and Y. Yoshida (1994), Seismic structure near the inner core-outer core boundary, *Geophys. Res. Lett.*, *21*, 157–160.

Kennett, B. L. N., E. R. Engdahl, and R. Buland (1995), Constraints on seismic velocities in the Earth from travel times, *Geophys. J. Int.*, *122*, 108–124.

Koper, K. D., and M. Dombrovskaya (2005), Seismic properties of the inner core boundary from *PKiKP/P* amplitude ratios, *Earth Planet. Sci. Lett.*, *237*, 680–694.

Koper, K. D., J. Franks, and M. Dombrovskaya (2004), Evidence for small-scale heterogeneity in Earth's inner core from a global study of *PKiKP* coda waves, *Earth Planet. Sci. Lett.*, *228*, 227–241.

Krasnoshchekov, D. N., P. B. Kaazik, and V. M. Ovtchinnikov (2005), Seismological evidence for mosaic structure of the surface of the Earth's inner core, *Nature*, *435*, 483–487.

Lay, T., J. Hernlund, E. Garnero, and M. S. Thorne (2006), A post-perovskite lens and D'' heat flux beneath the central Pacific, *Science*, *314*, 1272–1276.

Leyton, F., and K. D. Koper (2007), Using PKiKP coda to determine inner core structure: 2. Determination of Q_c, *J. Geophys. Res.*, *112*, B05317, doi:10.1029/2006JB004370.
Li, X., and V. F. Cormier (2002), Frequency dependent attenuation in the inner core: Part I. A viscoelastic interpretation, *J. Geophys. Res.*, *107*(B12), 2361, doi:10.1029/2002JB001795.
Loper, D. E. (1978), Some thermal consequences of a gravitationally powered dynamo, *J. Geophys. Res.*, *83*, 5961–5970.
Loper, D. E., and P. Roberts (1978), On the motion of an iron-alloy core containing a slurry. I. General theory, *Geophys. Astrophys. Fluid Dyn.*, *9*, 289–321.
Loper, D. E., and P. H. Roberts (1981), A study of the conditions at the inner core boundary of the Earth, *Phys. Earth Planet. Inter.*, *24*, 302–307.
Menke, W. (1982), On extending Biot's theory of multiple scattering at low frequencies from acoustic to elastic media, *Geophys. J. R. Astron. Soc.*, *69*, 819–830.
Menke, W. (1989), *Geophysical Data Analysis: Discrete Inverse Theory*, pp. 96–97, Academic Press, San Diego, Calif.
Nakanishi, I. (1990), High-frequency waves following PKP_{Cdiff} at distances greater than 155°, *Geophys. Res. Lett.*, *17*, 639–642.
Niu, F., and L. Wen (2001), Hemispherical variations in seismic velocity at the top of the Earth's inner core, *Nature*, *410*, 1081–1084.
Phinney, R., and S. S. Alexander (1966), P wave diffraction theory and the structure of the core-mantle boundary, *J. Geophys. Res.*, *71*, 5959–5975.
Poupinet, G., and B. L. N. Kennett (2004), On the observation of high frequency *PKiKP* and its coda in Australia, *Phys. Earth Planet. Inter.*, *146*, 497–511.
Qamar, A. (1973), Revised velocities in the Earth's core, *Bull. Seismol. Soc. Am.*, *63*, 1073–1105.
Rawlinson, N., and B. Kennett (2004), Rapid estimation of relative and absolute delay times across a network by adaptive stacking, *Geophys. J. Int.*, *157*, 332–340.
Resovsky, J., J. Trampert, and R. D. van der Hilst (2005), Error bars for the global seismic Q profile, *Earth Planet. Sci. Lett.*, *230*, 413–423.
Rial, J. A., and V. F. Cormier (1980), Seismic waves at the epicenter's antipode, *J. Geophys. Res.*, *85*, 2662–2668.
Ruff, L. J., and D. V. Helmberger (1982), The structure of the lowermost mantle determined by short-period P-wave amplitudes, *Geophys. J. R. Astron. Soc.*, *68*, 95–119.
Sacks, I. S., and G. Saa (1969), The structure of the transition zone between the inner core and the outer core, *Year Book Carnegie Inst. Washington*, *69*, 419–426.
Schulitz, F., Y. Lu, and H. Wadley (1998), Ultrasonic metal powder-viscous liquid suspensions, *J. Acoust. Soc. Am.*, *103*, 1361–1369.
Shearer, P. (1994), Constraints on inner core anisotropy from *PKP* (*DF*) travel times, *J. Geophys. Res.*, *99*, 19,647–19,659.
Shimizu, H., J. P. Poirier, and J. L. L. Mouel (2005), On crystallization at the inner core boundary, *Phys. Earth Planet. Inter.*, *151*, 37–51.
Song, X., and D. V. Helmberger (1992), Velocity structure near the inner core boundary from waveform modeling, *J. Geophys. Res.*, *97*, 6573–6586.
Song, X., and D. V. Helmberger (1995), A P wave velocity model of Earth's core, *J. Geophys. Res.*, *100*, 9817–9830.
Song, X., and P. G. Richards (1996), Observational evidence for differential rotation of the Earth's inner core, *Nature*, *382*, 221–224.
Souriau, A., and G. Poupinet (1991), The velocity profile at the base of the liquid core from *PKP* (*BC* + *Cdiff*) data: An argument in favor of radial inhomogeneity, *Geophys. Res. Lett.*, *18*, 2023–2026.
Souriau, A., and P. Roudil (1995), Attenuation in the uppermost inner core from broad-band GEOSCOPE PKP data, *Geophys. J. Int.*, *123*, 572–587.
Stroujkova, A., and V. F. Cormier (2004), Regional variations in the uppermost 100 km of the Earth's inner core, *J. Geophys. Res.*, *109*, B10307, doi:10.1029/2004JB002976.
Tanaka, S. (2005), Characteristics of PKP_{Cdiff} coda revealed by small-aperture seismic arrays: Implications for the study of the inner core boundary, *Phys. Earth Planet. Inter.*, *153*, 49–60.
Tichelaar, B. W., and L. J. Ruff (1989), How good are our best models? Jacknifing, bootstrapping, and earthquake depth, *Eos Trans. AGU*, *70*, 605–606.
Valenzuela, R. W., and M. Wysession (1998), Illuminating the base of the mantle with diffracted waves, in *The Core-Mantle Boundary Region*, *Geodyn. Ser.*, vol. 28, pp. 57–71, AGU, Washington, D. C.
van Decar, J. C., and R. Crosson (1990), Determination of teleseismic relative phase arrival times using multi-channel cross-correlation and least squares, *Bull. Seismol. Soc. Am.*, *80*, 150–159.
Vidale, J. E., and P. Earle (2000), Fine-scale heterogeneity in the Earth's inner core, *Nature*, *404*, 273–275.
Vinnik, L., B. Romanowicz, and L. Bréger (1994), Anisotropy in the center of the inner core, *Geophys. Res. Lett.*, *21*, 1671–1674.
Wen, L. (2006), Localized temporal change of the Earth's inner core boundary, *Science*, *314*, 967–970.
Wen, L., and F. Niu (2002), Seismic velocity and attenuation structures in the top of the Earth's inner core, *J. Geophys. Res.*, *107*(B11), 2273, doi:10.1029/2001JB000170.
Wessel, P., and W. Smith (1991), Free software helps map and display data, *Eos Trans. AGU*, 72, 441, 445–446.
Yu, W., and L. Wen (2006), Seismic velocity and attenuation structures in the top 400 km of the Earth's inner core along equatorial paths, *J. Geophys. Res.*, *111*, B07308, doi:10.1029/2005JB003995.
Yu, W., L. Wen, and F. Niu (2005), Seismic velocity structure in the Earth's outer core, *J. Geophys. Res.*, *110*, B02302, doi:10.1029/2003JB002928.
Zhu, L., and L. Rivera (2002), A note on the dynamic and static displacements from a point source in multi-layered media, *Geophys. J. Int.*, *148*, 619–627.
Zou, Z., F. Leyton, and K. D. Koper (2007), Partial melt in the lowermost mantle near the base of a plume, *Geophys. J. Int.*, *168*, 809–817.

V. F. Cormier, Department of Physics, University of Connecticut, 2152 Hillside Road, U-3046 Storrs, CT 06269-3046, USA.

K. D. Koper and Z. Zou, Department of Earth and Atmospheric Sciences, Saint Louis University, 3642 Lindell Boulevard, O'Neil Hall Room 201, St. Louis, MO 63103, USA. (zouz@eas.slu.edu)